Advanced DSP for 400 Gb/s and Beyond Optical Networks

Xiang Zhou and Lynn Nelson

(Invited Paper)

***Abstract*—This paper presents a systematic review of several digital signal processing (DSP)-enabled technologies recently proposed and demonstrated for high spectral efficiency (SE) 400 Gb/s–class and beyond optical networks. These include 1) a newly proposed SE-adaptable optical modulation technology—time-domain hybrid quadrature amplitude modulation (QAM), 2) two advanced transmitter side digital spectral shaping technologies—Nyquist signaling (for spectrally-efficient multiplexing) and digital pre-equalization (for improving tolerance toward channel narrowing effects), and 3) a newly proposed training-assisted two-stage carrier phase recovery algorithm that is designed to address the detrimental cyclic phase slipping problem with minimal training overhead. Additionally, this paper presents a novel DSP-based method for mitigation of equalizer-enhanced phase noise impairments. It is shown that performance degradation caused by the interaction between the long-memory chromatic dispersion compensating filter/equalizer and local oscillator laser phase noise can be effectively mitigated by replacing the commonly used fast single-tap phase-rotation-based equalizer (for typical carrier phase recovery) with a fast multi-tap linear equalizer. Finally, brief reviews of two high-SE 400 Gb/s-class WDM transmission experiments employing these advanced DSP algorithms are presented.**

***Index Terms*—Carrier recovery, clock recovery, coherent, digital signal processing (DSP), equalization, equalizer-enhanced phase noise, fiber, hybrid QAM, modulation format, nyquist, optical transmission, phase recovery, pulse shaping, quadrature amplitude modulation (QAM), spectral efficiency (SE).**

I. Introduction

HISTORICALLY it has been shown that increasing both per channel data rate and SE effectively reduces the transport cost. With commercial deployment of 100 Gb/s technology operating at 2 bit/s/Hz, research is shifting to the next generation of transport interface rate operating at even higher SE. The IEEE has recently launched a study group to explore development of a 400 Gb/s Ethernet standard. With 400 Gb/s being expected to be the next standard interface rate, several technology options for spectrally-efficient 400 Gb/s transmission have been experimentally explored [1]–[12], including the use of unconventional channel spacings to maximize the SE [3], [11], [12], in anticipation of the use of flex-grid reconfigurable optical add/drop multiplexers (ROADMs). However, the ability to place 400 Gb/s signals on the conventional 50 GHz or 100 GHz channel grid has advantages in terms of network management, and may be most cost-effective, as it could allow increasing the network capacity through upgrade of current ITU-T grid-based optical networks to 400 Gb/s per channel.

Several recently demonstrated experiments have revealed that, by using advanced digital signal processing (DSPs)-enabled technologies and in combination with low-noise all-Raman amplification and low-nonlinearity ultra-large area fiber, 400 Gb/s per channel signals can be transmitted over $>$3000 km with 50 GHz channel spacing [9], and over 12 000 km with 100 GHz channel spacing [10], at net SE of 8 and 4 bit/s/Hz, respectively.

This paper intends to provide a comprehensive review of the enabling DSPs used in those experiments, including 1) a newly proposed SE-adaptable optical modulation technology—time-domain hybrid quadrature amplitude modulation (QAM), 2) two advanced transmitter side digital spectral shaping technologies—Nyquist pulse shaping and digital pre-equalization, and 3) a training-assisted two-stage carrier phase recovery algorithm that is designed to address the detrimental cyclic phase slipping problem with minimal training overhead. In addition, this paper also presents a new method for mitigating equalizer-enhanced phase noise impairments. Through numerical simulation, we show that the impairments caused by the interaction between the long-memory dispersion-compensating filter/equalizer and local oscillator (LO) phase noise can be effectively mitigated by appropriately modifying the carrier recovery DSP.

The remainder of this paper is organized as follows. In Section II we focus on the SE-adaptable time-domain hybrid QAM that is enabled by the use of both transmitter side and receiver side DSP. Advanced digital spectral shaping techniques and the newly proposed training-assisted two-stage carrier phase recovery algorithm are presented in Sections III and IV, respectively. In Section V we describe a new method for mitigating equalizer-enhanced phase noise impairments. Two high-SE 400 Gb/s-class WDM transmission experiments enabled by these advanced DSP algorithms are described in Section VI. The conclusions are drawn in Section VII.

II. Time-Domain Hybrid QAM

High-order QAM formats such as 8 QAM, 16 QAM, 32 QAM and 64QAM have recently been experimentally explored for high-SE 400 Gb/s-class transmission. However, these regular 2^m-ary QAM systems may not be optimal for a 400 Gb/s

Manuscript received February 27, 2014; revised April 1, 2014; accepted April 20, 2014. Date of publication May 4, 2014; date of current version July 25, 2014.

X. Zhou was with the AT&T Labs, Middletown, NJ 07748 USA. He is currently with Google Inc., Mountain View, CA 94043 USA (e-mail: zhoux@google.com).

L. Nelson is with the AT&T Labs, Middletown, NJ 94043 USA (e-mail: ln4395@att.com).

Color versions of one or more of the figures in this paper are available online at http://ieeexplore.ieee.org.

Digital Object Identifier 10.1109/JLT.2014.2321135

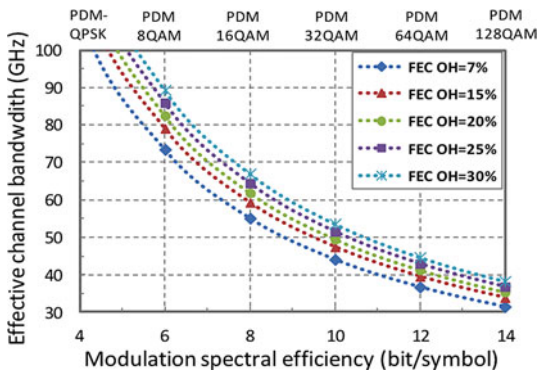

Fig. 1. Effective channel bandwidth versus modulation SE at several FEC code rates for a 400GigE system [9].

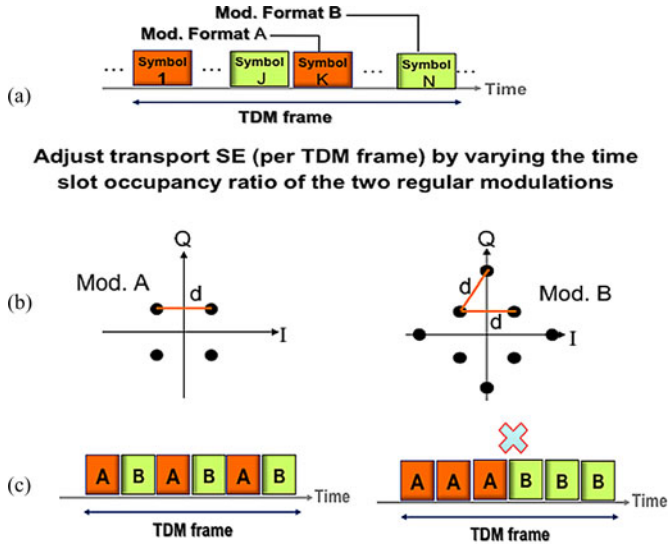

Fig. 2. Schematic illustration of the proposed time-domain hybrid QAM technique. (a) Concept of time-domain hybrid QAM; (b) equal Euclidean distance design concept for optimal linear performance and (c) uniform symbol distribution design concept for optimal nonlinear performance.

system operating on a 50 GHz or 100 GHz grid, as can be seen from Fig. 1, which plots the effective required channel bandwidth for regular $2^m - \text{ary}$ QAM formats at several different forward error correction (FEC) code rates for a 400GigE system. One can see that regular polarization-division-multiplexed (PDM) 8 QAM, 16 QAM, 32 QAM, and 64 QAM (with 6, 8, 10, and 12 bits/symbol, respectively) allow only certain effective channel bandwidths for a specific FEC code rate.

For a given channel bandwidth and FEC code rate, the performance of a 400 Gb/s system (or beyond) can be improved by using time-domain hybrid-QAM, a SE-adaptable modulation technique that is enabled by the use of both transmitter-side and receiver side DSP [8], [13]. For this technique, two regular $2^m - \text{ary}$ QAMs with different SE (in terms of bit/symbol) are assigned to different time slots within each TDM frame as is shown in Fig. 2, where the two QAMs are denoted as modulation A and B, respectively. Any SE (per TDM frame) that falls between the SE of the two regular QAMs can be realized by appropriately designing the TDM frame length and the time slot occupancy ratio of the two QAMs. To achieve an optimal linear performance (i.e. additive noise tolerance performance), the Euclidean distance of modulation A and modulation B should be designed to be identical as is shown in Fig. 2(b), because an equal Euclidean distance design will result in identical noise tolerance for the two different modulation formats. To achieve an optimal nonlinear performance for a long-distance transmission system without using inline optical dispersion compensation, the symbols of modulation A and modulation B should be distributed as uniformly as possible within each TDM frame, as is shown in the left figure of Fig. 2(b). For comparison, grouping all the same modulation symbols (within each TDM frame) together [see the right figure of Fig. 2(c)] will result in worse nonlinear performance [14], [15]. The reason is that the use of equal Euclidean distance design will result in higher average power for the higher-order modulation symbols. Locating all the higher average-power symbols (belonging to each TDM frame) together will result in higher local average power, thus reducing tolerance toward nonlinear effects.

Note that arbitrary SE also can be achieved by using an orthogonal frequency division multiplexing (OFDM) based hybrid QAM technique [6], [16]. Compared to such a frequency-domain-based method, time-domain hybrid QAM exhibits several potential advantages, such as lower peak-to-average power ratio (PAPR) [17] and better tolerance toward laser phase noise due to the fundamentally shorter symbol period. These two advantages could be important for high-SE optical communication systems where, in addition to additive Gaussian noise, fiber nonlinear effects and laser phase noise also are major performance limiting factors. Although the higher PAPR of OFDM is less of a concern (in terms of nonlinear tolerance) for ultra-long-haul systems using no inline dispersion compensation [18], the higher PAPR may still be a problem for metro/regional systems, which have shorter transmission reach, or legacy line systems utilizing inline optical dispersion compensation.

Non-regular modulation SE also can be realized by using some multidimensional-constellation-based coding technologies [19], [20]. For example, compared to the conventional mapping of multiple binary bits into one symbol, one can map multiple binary bits into multiple symbols to achieve non-integer average binary bits per symbol. Through optimal decoding techniques, multidimensional-constellation based modulation formats, in principle, can achieve better performance than the time-domain hybrid QAM. But the required implementation complexity may be a problem, if the required mapping dimension is high. For example, if we want to achieve a SE of 8.2 bit/s/Hz per symbol, then we may have to map 41 binary bits into five 294-ary symbols (each symbol to carry 8.2 bits on average), resulting in a constellation size of $294^5 (> 2.12e + 12)$. Optimal decoding for such a large constellation size can be difficult, although some simpler sub-optimal solutions may exist. On the contrary, the implementation complexity for the proposed time-domain hybrid QAM can remain low for any SE because it does not increase mapping dimensions.

The capability of arbitrary SE also may be realized by using some code-rate-adaptable FEC schemes [21]. With the same modulation format, the effective SE can be adjusted by changing the code rate of the used FEC. However, in order to achieve

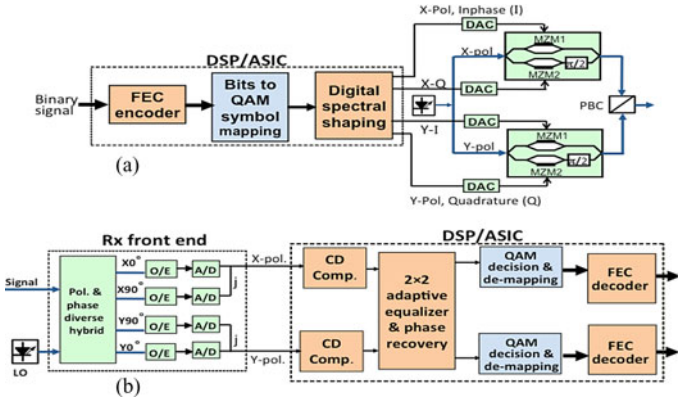

Fig. 3. Schematic illustration of (a) transmitter (b) and receiver functional blocks for generating and receiving time-domain hybrid QAM.

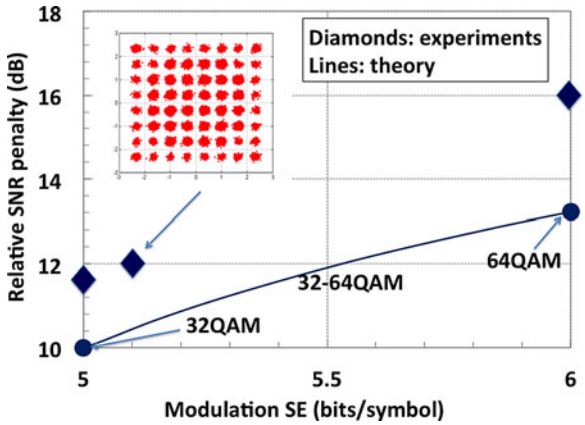

Fig. 5. Back-to-back SNR penalties for 32QAM, hybrid 32–64QAM and 64QAM, all operating at 9.7Gbaud and relative to theoretical QPSK sensitivity.

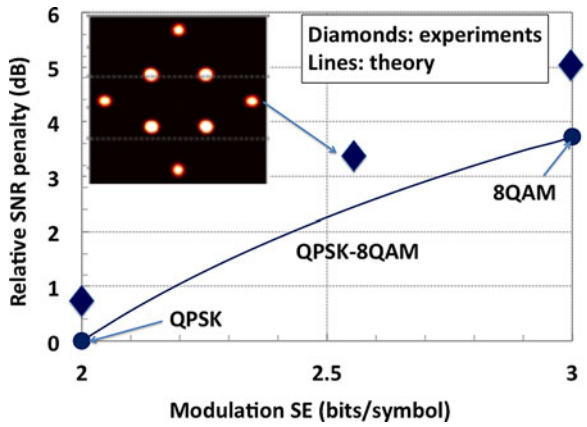

Fig. 4. Back-to-back SNR penalties for QPSK, hybrid QPSK-8QAM, and 8QAM, all operating at 9.7Gbaud and relative to theoretical QPSK sensitivity.

rate-adaptable capability, the FEC performance usually has to be compromised. For real-world applications, more studies are needed to understand the performance and implementation complexity trade-offs between code-rate-adaptable FEC techniques and the time-domain hybrid QAM technique.

Compared to conventional systems using regular QAMs, the time-domain hybrid QAM only requires a slight modification of the bits-to-symbols mapping functional block at the transmitter [see Fig. 3(a)] and the symbol-to-bits mapping functional block at the receiver [see Fig. 3(b)]. Due to this significant implementation advantage, time-domain hybrid QAM could be a good candidate for realizing a fine-granularity rate-adaptable transponder [14], [22]. Recently it has been shown that, through channel-by-channel capacity/SE optimization, the use of fine-granularity rate-adaptable transponders could enable us to reduce the network transport cost by up to 30% for a realistic reach-diverse long-haul optical network [22].

The proposed time-domain hybrid QAM has been experimentally demonstrated at different net SEs. Fig. 4 shows the measured back-to-back results for using regular QPSK, 8QAM and hybrid QPSK operating at 9.7Gbaud. For the hybrid QPSK-8QAM, each TDM frame consists of 128 symbols, where 77 symbols are 8QAM and 48 are QPSK. The extra 3 symbols are used as training symbols for carrier phase recovery, resulting in a net modulation SE of 2.55 bits per symbol. The measured results are shown as symbols in Fig. 4. For comparison, the theoretical prediction is shown as a solid line. From this measurement, the hybrid QPSK-8QAM is about 1 dB better than the regular 8QAM, which agrees with the theoretical prediction. The inset of Fig. 4 shows the measured constellation diagram of hybrid QPSK-8QAM. The use of equal Euclidean distance design results in an 8QAM-like constellation with un-equal constellation occupation probability: the outer four constellation points have fewer symbols than the inner four constellation points. Such a hybrid QPSK-8QAM is found to be optimal for operating 400 Gb/s system over 100 GHz WDM grid using 20% FEC overhead and is one of the key enablers for our recent record-breaking 400 Gb/s class transmission experiment: 8×495 Gb/s over 120 000 km using the standard 100 GHz ITI-T WDM grid [10], where 10 subcarriers are used to create each 495 Gb/s per channel signal.

Fig. 5 shows the measured back-to-back results for regular 32QAM, 64QAM and hybrid 32–64QAM, also operating at 9.7Gbaud. For the hybrid 32–64QAM signals, each TDM frame consists of 128 symbols, where 28 symbols are 64QAM and 97 are 32QAM. The extra 3 symbols are used as training symbols for carrier phase recovery, resulting in a net SE of 5.1 bit/s/Hz. The 64QAM symbols are uniformly distributed within each TDM frame. This hybrid 32–64QAM enables generation of a 495 Gb/s signal (including 20% FEC overhead) using only 48.5 GHz optical bandwidth, which can be placed into a 50G Hz channel grid [9]. As compared to the regular 64QAM, this hybrid 32–64QAM improves the SNR (signal-to-noise ratio) sensitivity by 2.3 dB.

III. Transmitter Side Digital Spectral Shaping

50 GHz-spaced 100 Gb/s transport systems are basically enabled by the use of coherent detection and receiver-side DSP. For a 400 Gb/s system operating at a higher SE, transmitter-side DSP also could become indispensable. Transmitter-side DSP enables the realization of flexible modulation, such as the time-domain hybrid QAM described before, as well as several critical

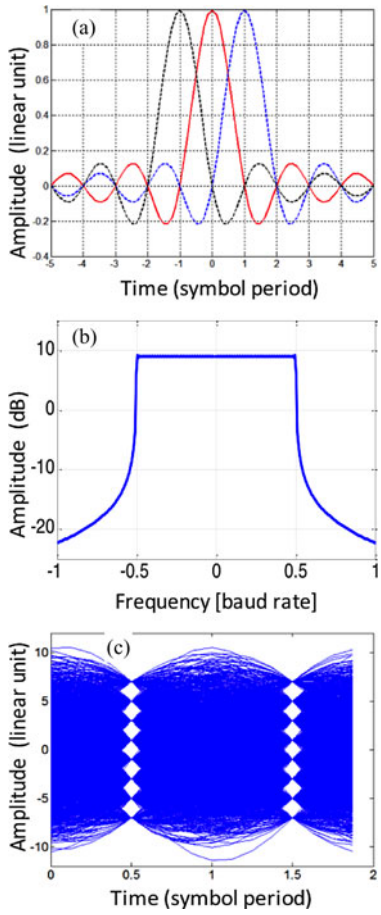

Fig. 6. Simulations of Nyquist pulse signaling: (a) illustration of three Nyquist pulses in the time domain; (b) frequency-domain spectrum with roll-off factor = 0.01 and (c) eye diagram of a Nyquist-shaped 32–64 hybrid QAM signal.

spectral shaping techniques [23], including Nyquist pulse shaping and digital pre-equalization.

Nyquist signaling is also known as an orthogonal time-division-multiplexing technique, because although each symbol pulse spreads into many adjacent time slots, no ISI occurs if the sampling is performed at the center of each symbol due to the nature of sinc-shaped pulses, as can be seen from the simulation in Fig. 6(a). Nyquist signaling can achieve the highest SE for any given modulation format, because the spectrum has very sharp rising/falling edges. A square spectrum occupying a bandwidth equal to the baud rate can be achieved by using a raised-cosine pulse with a frequency-domain roll-off factor equal to 0. For any practical Nyquist signaling with non-zero roll-off factor, the signal will occupy an extra-bandwidth equal to the product of the roll-off factor and the signal symbol rate. In Fig. 6(b) we show the calculated spectrum of a raised-cosine signal with a roll-off factor equal to 0.01. Due to the nearly square spectrum, Nyquist signaling allows multiple WDM channels or multiple sub-channels to be closely packed (to increase WDM SE) without using tight optical filtering. Using an OFDM-based technique also can generate nearly square spectra, but an OFDM-modulated signal inherently exhibits a higher PAPR and is also less tolerant to laser phase noise due to the long symbol period.

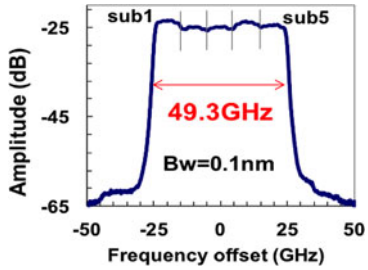

Fig. 7. Optical spectrum of a 495 Gb/s PDM hybrid 32–64QAM signals generated using five subcarriers.

In Fig. 6(c) we show a simulated eye diagram for a Nyquist-shaped 9Gbaud time-domain 32–64 hybrid QAM signal with a roll off factor equal to 0.01. One can see that a Nyquist-shaped signal has very small eye openings, indicating that it is inherently vulnerable to clock timing errors. But such a problem can be effectively mitigated by using fast digital equalization algorithms that have already been widely adopted in today's digital coherent optical communication systems. In order to achieve the best noise tolerance, the Nyquist signaling filter $H(f)$ can be divided into two identical filters, $\sqrt{H(f)}$, with one being implemented at the transmitter as a pulse shaping filter and a second being implemented at the receiver as a matched receiving filter.

Transmitter-side pre-equalization can be used for pre-compensation of the band-limiting effects caused by the D/A converters and the IQ modulators, as well as the narrow filtering effects from wavelength routing devices such as ROADMs. For transmitter-side band-limiting effects, pre-equalization performs better than post-transmission equalization, because post-equalization will enhance the noise components [24]. For distributed band-limiting effects caused by ROADMs, joint pre- and post-transmission equalization should perform better than post-transmission-only equalization.

Fig. 7 shows the measured optical spectrum of a 495 Gb/s PDM hybrid 32–64QAM signal generated by using five frequency-locked subcarriers (subcarrier spacing 9.9 GHz, symbol rate per subcarrier 9.7Gbaud) [9], where close to ideal digital Nyquist pulse shaping (roll-off factor = 0.01) was used to confine the optical spectrum to be within 49.3 GHz and digital pre-equalization was used to reduce the implementation penalty (from the transmitter band-limiting effects). With a guard-band of only 200 MHz between two adjacent subcarriers, the measured inter-subcarrier crosstalk is still smaller than 0.2 dB at bit-error-ratio (BER) of 2×10^{-2} (see Fig. 8).

Nyquist pulse shaping, digital pre-equalization as well as fiber dispersion pre-compensation all can be implemented in the frequency domain by using a single digital spectral-shaping filter [see Fig. 3(a)]. The reception of a Nyquist-shaped signal requires a longer receiving filter (i. e. the matched filter) for optimal performance. To reduce the receiver implementation complexity, one can divide the receiving filter into two parts, a long, matched static filter followed by a short, regular adaptive filter, as is described in [25]. Note that the matched filter can share the same static filter used for the fiber dispersion post-compensation.

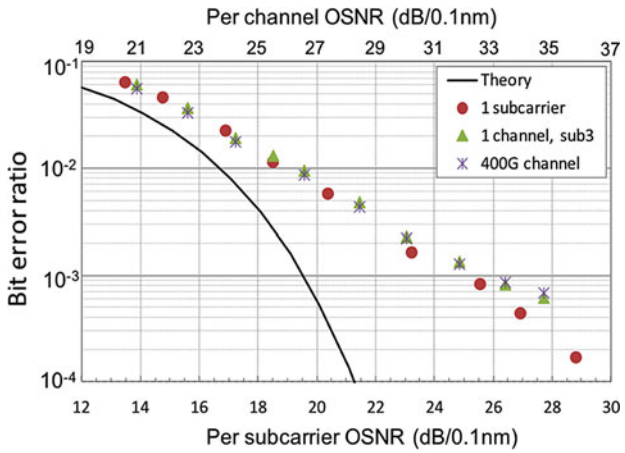

Fig. 8. Measured back-to-back BER performance versus OSNR under three different conditions for a 495 Gb/s PDM hybrid 32–64QAM signal consisting of five subcarriers.

The use of high-SE Nyqusit signaling requires re-design of the clock recovery circuit, because the classic Gardner timing error [26] detector as expressed in the following equation (1) could fail [17] when the Nyquist filter roll off factor is small (the clock tone completely disappears for an ideal Nyquist signal)

$$\tau_{\mathrm{err}} = \sum_{n=0}^{N/2-1} [x(2n-1) - x(2n+1)] \cdot x^*(2n). \qquad (1)$$

In equation (1), x (n) denotes a complex input sequence sampled at two samples per symbol, and $*$ denotes complex conjugation. Recently, a modified Gardner phase detector algorithm has been proposed for Nyquist-shaped signal [27], [28]. For this method, the phase error detector is given by

$$\tau_{\mathrm{err}} = \sum_{n=1}^{N/2} [P(2n+1) - P(2n-1)] \cdot P(2n) \qquad (2)$$

where P is the power of the received signal (assume two samples per symbols). It has been shown that such a modified timing error detector greatly improves the performance for a Nyquist-shaped signal. Alternatively, the standard deviation of the amplitude of the received signal also can be used as a measure of timing phase error [17] for Nyquist-shaped signals. For these modified algorithms aimed at Nyquist-shaped signals, more work needs to be done to understand their tolerance toward channel distortion.

IV. Training-Assisted Two-Stage Phase Recovery

For a coherent optical receiver, accurate and reliable carrier phase recovery is indispensable for demodulating any coherently modulated optical signals. Because high-speed DSP requires high-degree of parallel processing, feed-forward-based fast phase recovery algorithms are preferable for high-speed optical systems, especially if high-order modulation formats are employed. So far, several feed-forward-based blind phase recovery algorithms have been proposed, including the classic Viterbi-Viterbi based algorithms [29], the minimum mean square error based blind phase search (BPS) algorithm [30], the multi-stage hybrid BPS and maximum likelihood (ML) algorithm [31], and mutli-stage hybrid phase-locked-loop and ML algorithms [32].

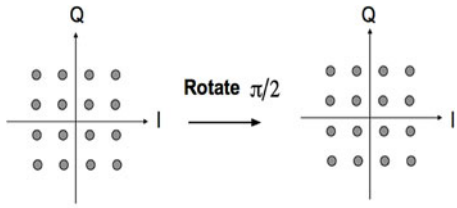

Fig. 9. Schematic illustration of cyclic phase slipping problem.

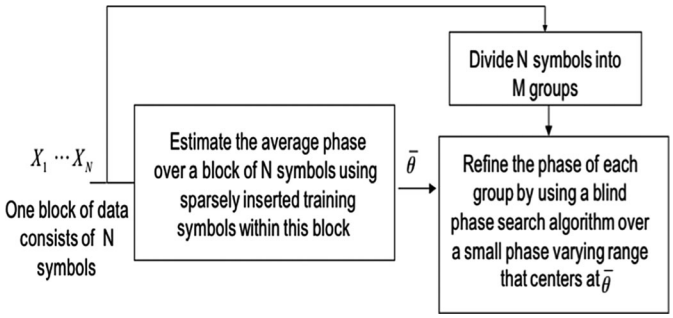

Fig. 10. Functional block illustration for the proposed phase recovery algorithm.

For these proposed blind phase recovery algorithms, however, differential coding and decoding is required to deal with the detrimental cyclic phase slipping problem. The cyclic phase slipping problem occurs if the signal constellation exhibits a certain degree of phase symmetry, which is the case for most of the QAMs, as is illustrated in Fig. 9, where a $\pi/2$ phase rotation of a 16QAM signal is still a 16QAM signal. With such phase symmetry, an accidental $\pi/2$ phase jump due to the impact of random noise or nonlinear phase noise could result in phase jumps for many of the following symbols, causing a long burst of errors.

Although differential coding/decoding is an effective method to address this problem, it will result in about 0.5 dB to 1 dB sensitivity penalty (depending on the chosen modulation format) for a system using a high coding gain FEC. To remove the need for differential coding and decoding and improve the receiver sensitivity, a new training-assisted two-stage phase recovery algorithm has recently been proposed and demonstrated [9]. This new algorithm could effectively mitigate the cyclic slipping problem by using a relatively small training overhead (around 2% or less). The functional block illustration of the proposed phase recovery algorithm is shown in Fig. 10. For this new method, training symbols that are known at the receiver are periodically inserted into the data stream to assist in the phase recovery. To reduce the training overhead, training symbols are only sparsely inserted at the transmitter. At the receiver, the received data is processed block by block, where each block contains at least two training symbols. For each block of data, first the average phase over this block is estimated by using the inserted training symbols through, for an example, the well-known ML based phase estimation method [33]. Second, each

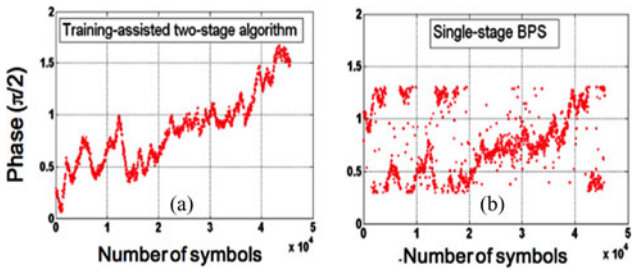

Fig. 11. Recovered carrier phases using two different algorithms: training – assisted two-stage algorithm and single-stage BPS algorithm, for a 400G WDM transmission experiment using a time-domain hybrid PDM-32–64QAM modulation format.

block is divided into multiple groups, and then the phase of each group is refined by using a BPS algorithm [30] over a small phase-varying range that is centered at the average phase estimated through the training symbols.

The validity of this new method has been verified by a 400 Gb/s experiment using a time-domain hybrid 32–64QAM modulation format [9]. This new algorithm is shown to be very robust against cyclic phase slipping or phase jumping, as is shown in Fig. 11, which displays the recovered carrier phases using two different algorithms: the proposed training–assisted two-stage algorithm and the conventional BPS are displayed for a back-to-back measurement with OSNR = 24.2 dB (corresponding to a bit-error-ratio of 2e-2 when using the training-assisted algorithm). For the new algorithm, three training symbols are introduced for every 128 symbols, and the training symbols are uniformly distributed within each block. One can see that there was no phase jump when using the proposed training-assisted two-stage algorithm, whereas the phase-jump problem was severe when using the conventional single-stage BPS algorithm (due to low OSNR, non-ideal equalization, and imperfect signal constellation in this experiment), thus mandating the use of differential coding.

In terms of laser phase noise tolerance, this new two-stage algorithm is comparable to the single-stage BPS algorithm, but the implementation complexity is much lower. The required training overhead can be further reduced by exploring joint phase recovery over two orthogonal polarization states for current polarization multiplexed transmission systems or joint phase recovery over multiple spatial channels for future space division multiplexed systems [34].

V. Digital Mitigation of Equalizer Enhanced Phase Noise Impairments

The carrier phase recovery algorithms developed so far are mostly optimized based on the additive Gaussian noise assumption. The impact of a long-memory equalizer, such as the 1×1 chromatic dispersion (CD)-compensating filter and/or the multi-input multi-output equalizer-based large inter-modal dispersion compensator (in few-mode fiber based space division multiplexing systems), has not been considered in the design of carrier phase recovery.

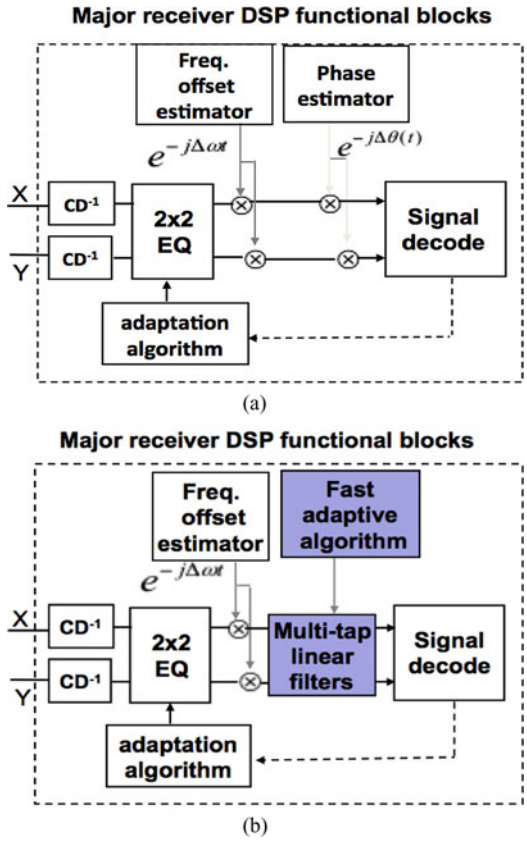

Fig. 12. Major receiver functional blocks for the conventional coherent receiver (a) and the proposed improved coherent receiver (b).

For the case with additive Gaussian noise, the phase noise from the signal source and the LO have essentially similar system impact, which can be minimized by using a fast single-tap-based phase rotation equalizer, as is shown in Fig. 12(a). For a coherent system using a long memory equalizer (assume to be employed at the receiver side) to compensate for the fiber dispersion, however, the impacts of signal and LO phase noise become quite different, because the signal source experiences both positive CD from the fiber and negative CD from the digital equalizer, but the LO only sees negative CD from the digital equalizer. Due to the fact that CD can convert phase noise into amplitude noise (and may also enhance phase noise), the impact of LO phase noise becomes significantly more severe than the signal source phase noise [35]–[37], and the additional amplitude distortion caused by a long-memory equalizer cannot be mitigated by using conventional phase recovery algorithms. It is also found that, the penalty from such an equalizer-phase noise interaction (EPNI) increases with the symbol rate [36] and can be a significant problem for future 400-Gb/s and beyond systems operating at very high baud rate. To address this problem, a hardware-based laser phase noise compensation method has recently been proposed [38]. However, this method is very complex and costly, because it requires an additional coherent receiver to measure the laser phase noise.

Here a purely DSP-based solution is proposed to address this challenge. The basic idea is based on the following observations: if the laser linewidth is small and signal baud rate is high,

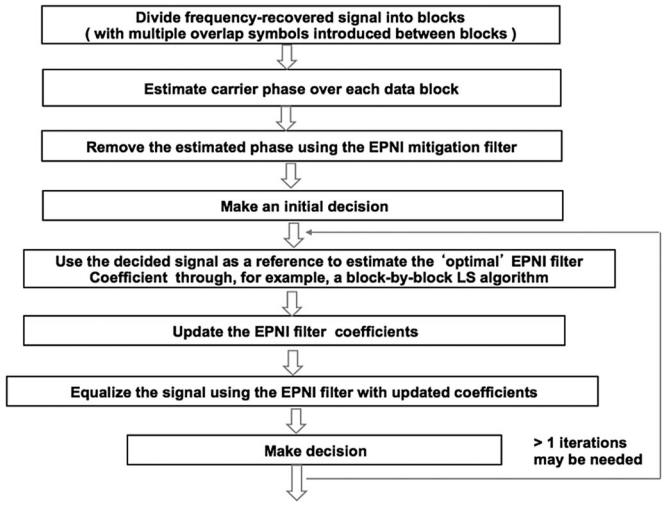

Fig. 13. Operational principle of the proposed EPNI mitigation method.

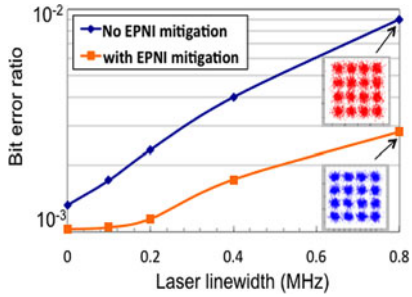

Fig. 14. Simulated BER performance vs. laser linewidth for a 7channel 49Gbaud PDM-16QAM WDM system (at 3dBm launch power and 2000 km transmission of an ultra-large area fiber) with and without using the proposed EPNI mitigation technology.

the amplitude and phase distortions caused by EPNI will be highly-correlated over quite a few symbols (tens to hundreds of symbols depending on the laser linewidth and the symbol rate), and more over, such distortions can be modeled as the result of a time-varying multi-tap linear filtering effect where, although the filter coefficients change over time, over every limited time block (consisting of tens to hundreds of symbols), the filter coefficients can be well approximated as unvarying constants. Thus, by replacing the commonly used fast-tracking single-tap phase rotation equalizer with a fast-tracking multi-tap linear equalizer, as is shown in Fig.12(b), both the amplitude and phase distortion caused by EPNI can be mitigated.

Because laser phase noise typically varies 2 to 4 orders of magnitude faster than the state of polarization change, the adaption rate for the proposed EPNI mitigation equalizer should be much faster than the regular polarization equalizer. Very fast adaptation rate can be realized by using feed-forward-based adaptation algorithms, for example, the classic block-by-block least-squares (LS) based algorithms. To reduce the impact of imperfect decision accuracy, multiple iterations may be applied to each data block for filter coefficients update, as is shown in Fig. 13. The initial decision is made based on performing pure phase recovery over the current data block. But the initial decision may also be made by applying the recovered phase of the prior data block to the current data block or by directly applying the EPNI filter coefficients acquired from the prior data block to the current data block (the starting phase or EPNI filter coefficients can be obtained using a starting training sequence). Because the block length cannot be too large due to the need of rapid adaption and the time-varying nature of EPNI, the accumulated amplifier noise may degrade the performance of the proposed EPNI equalizer. This problem may be alleviated by joint optimization of the proposed EPNI filter over both polarizations, because the phase noises in X- and Y-polarizations are usually correlated (typically they are from the same source).

The proposed new impairment mitigation method has been numerically verified for a 7-channel 50 GHz-spaced 49Gbaud PDM-16QAM system (operating at 392-Gb/s per channel bit rate, with Nyquist pulse shaping using a roll off-factor of 0.01) by using a block-by-block iterative LS algorithm. The transmission link consists of 20 total spans composed of 100 km of large area fiber (dispersion coefficient and fiber loss are assumed to be 21 ps/nm/km and 0.18 dB/km, respectively) and EDFA-only amplification (noise figure is assumed to be 5 dB). No in-line optical dispersion compensation is used for this simulation. For simplicity, polarization-mode dispersion and polarization-dependent loss are not considered in this simulation. For the laser sources, we assume that the signal source and the LO have identical linewidth.

Fig. 14 shows the BER performance of the middle channel (ch.4) versus the laser linewidth at the optimal signal launch power 3 dBm/channel. The diamonds-shaped symbols give the results using a conventional coherent receiver, where the phase is tracked by using the previously described training-assisted two-stage phase recovery algorithm. (The phase is firstly estimated by using three training symbols that are uniformly distributed over every 128 symbols, and then the 128 symbols are divided into four groups and the phase over each group is refined by using a blind phase recovery algorithm [30] over a small phase varying region.) The square-shaped symbols give the result using the proposed EPNI mitigation method, where a 5-tap T_s-spaced (T_s denotes the symbol period) 1×1 linear equalizer operating with a block-by-block adaptive LS algorithm is used for each polarization for simultaneous phase recovery and additional EPNI distortion mitigation. For this study, the block length is chosen to be 95 symbols (including 5 overlap symbols), and two iterations are applied for each data block, where the initial decision for each data block is made based on the same phase recovery algorithm used for the conventional coherent receiver (i.e. for the diamond-shaped symbols).

The effectiveness of the proposed algorithm is evident from Fig. 14. For a laser linewidth 0.8 MHz (a typical linewidth for widely used DFB lasers), the new method improves the Q performance by 1.35 dB by using only two iterations. As we further increase the number of iterations, the performance gain is small, as can be seen from Table I. It is interesting to note that, even without laser phase noise, the introduction of a five-tap EPNI equalizer improves the performance by 0.22 dB, indicating that the proposed method also helps in mitigating fiber nonlinear effects. To confirm this, we also simulated the results

TABLE I
SIMULATED BER VERSUS NUMBER OF ITERATIONS (LASER LINEWIDTH = 0.8 MHZ) WHEN USING THE PROPOSED EPNI MITIGATION ALGORITHM

Iteration	0	1	2	3	4
BER	8.86e-3	3.56e-3	2.81e-3	2.67e-3	2.65e-3

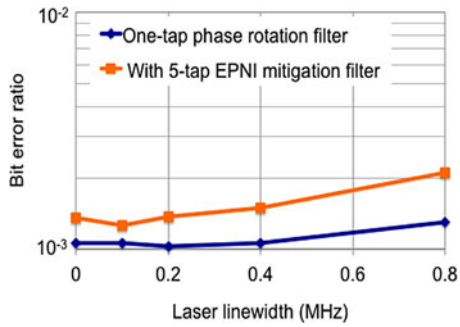

Fig. 15. Back-to-back performance comparison (OSNR = 23 dB) when using the conventional one-tap filter-based phase recovery method and the proposed multi-tap filter-based impairment mitigation method.

by switching off the fiber nonlinearity and found that the use of EPNI mitigation equalizer does not improve the performance. In fact, when the fiber nonlinearity is switched off, the use of EPNI mitigation equalizer slightly degrades the performance (BER = 2e – 5 versus BER = 1.8e – 5 when using the normal phase recovery algorithm).

A similar result is observed in our back-to-back simulations, as shown in Fig. 15. One can see that: 1) for conventional one-tap filter-based phase recovery, increasing the laser linewidth from 0 to 0.8 MHz only results in a small performance degradation when there is no EPNI effect; and 2) the use of the EPNI mitigation filter does not improve the performance when there are no EPNI effects. The small performance degradation caused by the EPNI mitigation filter when there are no EPNI effects (apparent in Fig. 15) probably occurs because the block length of 95 symbols is not long enough for optimal estimates of the five complex EPNI filter coefficients. (Note that the normal phase recovery only needs to estimate one real filter coefficient, the phase angle.)

VI. HIGH-SE 400 GB/S WDM EXPERIMENTS

A. 8.25 b/s/Hz, 3200 Km WDM Transmission [9]

By using PDM, time-domain hybrid 32–64QAM, close to ideal Nyquist pulse shaping, training-assisted two-stage carrier phase recovery and both pre- and post-transmission digital equalization, transmission of ten 494.85 Gbit/s DWDM signals on the standard 50 GHz ITU-T grid over 32×100 km of ultra-large-area (ULA) fiber has been successfully demonstrated. After excluding the 20% soft-decision FEC overhead, a net transport SE of 8.25 b/s/Hz, and SE distance product of 26 400 km.b/s/Hz was achieved.

To overcome the limitation of available digital-to-analog (D/A) converter bandwidth, five subcarriers were utilized to create the 494.85 Gb/s per-channel signal. The five frequency-locked subcarriers were generated from a single laser source by using two Mach-Zehnder modulators (MZMs), each driven with a 9.9 GHz clock, and followed by either a 12.5/25 GHz interleaver filter (ILF) or two cascaded 25/50 GHz ILFs, as shown in [9]. The odd and even subcarriers were modulated by two independent I/Q data modulators, each driven with a Nyquist-shaped 9.7Gbaud pre-equalized time-domain hybrid 32–64QAM (SE = 5.1 bit/symbol) signal, having 2^{15} pseudorandom pattern length.

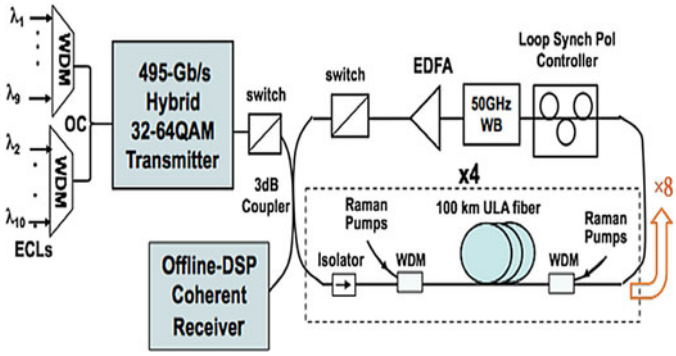

Fig. 16. 50 GHz-spaced,10 × 494.85 Gbit/s DWDM transmission setup,

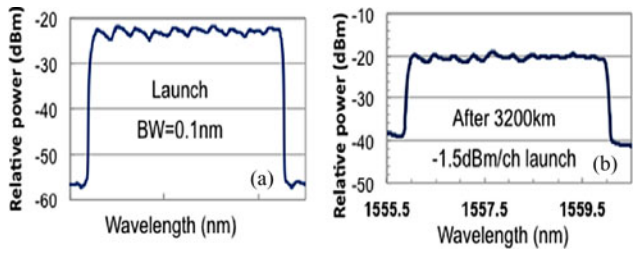

Fig. 17. Optical spectra measured prior to and after 3200 km transmission.

The recirculating-loop-based WDM transmission setup is shown in Fig. 16, where each loop consists of four 100-km spans of ULA fiber having, at 1550 nm, 135 um^2 average Aeff and 0.179 dB/km average attenuation. The spans are configured for all-Raman amplification, resulting in total span losses (fiber + components) of between 19.7 and 20.1 dB. For each span, counter-pumps at 1435 and 1455 nm with 310 and 650 mW, respectively, provide an average of 17 dB on-off Raman gain, while co-pumps at 1455 nm with 180 mW power provide an average of 3 dB on-off gain. After the last span, a loop-synchronous polarization controller is followed by a wavelength-blocker-based channel power equalizer.

The measured optical spectra prior to transmission and after 3200 km transmission are shown in Fig. 17(a) and (b), respectively. The measured BERs of all the ten WDM channels after 3200 k transmissions are shown in Fig. 18. The recovered constellation diagrams after 3200 k transmissions are also shown as insets.

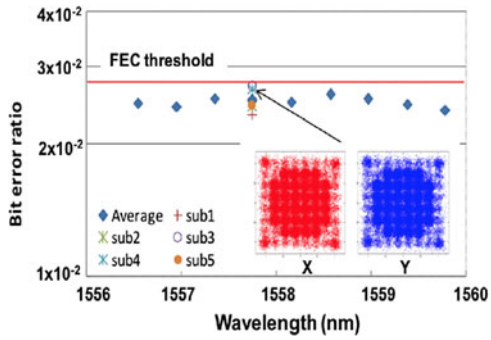

Fig. 18. Measured BER of ten 494.85 Gb/s DWDM channels after 3200 km transmission.

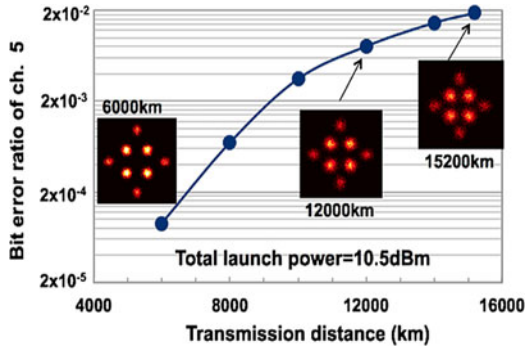

Fig. 19. 100 GHz-spaced, 8 × 495 Gb/s DWDM transmission results: Measured BER of a center channel (1556.6 nm) vs. distance.

B. 4 b/s/Hz, 12 000 Km WDM Transmission [10]

Just recently, we reported a record-breaking 12 000 km transmission of 100 GHz-spaced, 8 × 495 Gbits/s PDM QPSK-8QAM DWDM signals over ULA fiber at a net SE of 4.125 bit/s/Hz (after excluding the 20% soft-decision FEC overhead). Novel, improved carrier-phase recovery and equalization algorithms and time-domain hybrid QAM were key enablers. Compared to the prior 3200 km transmission of 495 Gb/s hybrid 32–64QAM signals, we gain 7.9 dB in OSNR sensitivity due to QPSK-8QAM and ∼1 dB due to the larger effective area (150 μm^2) and lower loss of the ULA fiber. After 12 000 km transmission, more than 1.5 dB Q margin was observed for all the eight channels. The resulting SE·distance product is 49 500 (bit/s/Hz)·km.

For this experiment, ten subcarriers are utilized to create each 495 Gb/s per-channel signal, as shown in [10]. Two 49.8 GHz spaced, narrow linewidth lasers are first combined and sent through a MZM driven with a 9.9 GHz clock, followed by an erbium-doped fiber amplifier (EDFA). After a 3 dB coupler, four subcarriers result after the 12.5/25 GHz ILF. Six additional subcarriers are generated by a second MZM also driven with a 9.9 GHz clock, followed by two cascaded 25/50 GHz ILFs. The two sets of subcarriers then are modulated by two independent I/Q data modulators, each driven with a Nyquist-shaped 9.7Gbaud pre-equalized time-domain hybrid QPSK-8QAM (SE = 2.5545 bit/symbol) signal, having 2^{15} pseudorandom pattern length.

The recirculating-loop based WDM transmission setup and the measured WDM spectra can be found in [10]. The measured BER of the middle channel vs. transmission reach is shown in Fig. 19, where the received constellation diagrams after 6000, 12 000 and 15 200 km are also shown as insets. The measured BER is still smaller than 2e-2 after 15 200 km transmission.

VII. Conclusion

We presented a systematic review of several advanced DSP techniques that have been proposed and demonstrated for 400 Gb/s and beyond optical networks. We have shown that time-domain hybrid QAM can be used to fine tune the spectral efficiency of the modulation format to optimize the transmission performance for specific channel bandwidth and FEC redundancy requirements. This technology also provides a new means to build fine-granularity rate-adaptable optical transponders, which can be used to perform channel-by-channel capacity/SE optimization to maximize the overall network capacity (thus reducing the cost per transmitted bit) for a reach-diverse network.

We showed that advanced digital spectral shaping technologies improves the performance of high-SE 400Gb/s-class transmission systems, and aggressive Nyquist signaling allows us to achieve spectrally efficient multiplexing without using optical filtering, and pre-transmission digital equalization performs better than post-transmission equalization for fighting transmitter side-band-limiting effects. Nyquist-pulse shaping and pre-equalization, as well as dispersion precompensation, can be implemented by a single digital spectral-shaping filter. However, at the receiver side, Nyquist pulse shaping requires modified clock recovery algorithms.

To increase the receiver sensitivity, we introduced a new training-assisted two-stage carrier recovery algorithm. This algorithm effectively mitigates the detrimental cycle slipping problem, enabling up to 1 dB receiver sensitivity improvement by removing the need for differential coding and decoding.

We also described a novel DSP-based method for mitigation of equalizer-enhanced phase noise impairments. Through numerical simulation we showed that the performance degradation caused by the interaction between the long-memory dispersion-compensating filter and LO phase noise can be effectively mitigated by replacing the commonly used fast single-tap phase rotation equalizer (for typical carrier phase recovery) with a fast multi-tap linear equalizer.

Finally, we presented a brief review of two high-SE 400 Gb/s-class WDM transmission experiments recently demonstrated and enabled by the use of advanced DSP techniques.

References

[1] X. Liu, S. Chandrasekhar, B. Zhu, A. H. Gnauck, and D. W. Peckham, "Transmission of a 448-Gb/s reduced-guard-interval CO-OFDM signal with a 60-GHz optical bandwidth over 2000 km of ULAF and five 80-GHz-Grid ROADMs," presented at the Opt. Fiber Commun. Conf. Expo./Nat. Fiber Opt. Eng. Conf., San Diego, CA, USA, Mar. 2010, Paper PDPC2.

[2] J. Yu, X. Zhou, M. Huang, D. Qian, P. N. Ji, T. Wang, and P. D. Magill, "400 Gb/s (4 × 100 Gb/s) orthogonal PDM-RZ-QPSK DWDM signal

transmission over 1040 km SMF-28," *Opt. Exp.*, vol. 17, no. 20, pp. 17928–17933, 2009.

[3] Y.-K. Huang, E. Ip, M.-F. Huang, B. Zhu, P. N. Ji, Y. Shao, D. W. Peckham, R. LingleJr, Y. Aono, T. Tajima, and T. Wang, "10×456-Gb/s DP-16QAM transmission over 8×100 km of ULAF using coherent detection with a 30-GHz Analog-to-Digital Converter," presented at the OptoElectron. Commun. Conf., Sapporo, Japan, Jul. 2010, Paper PDP3.

[4] P. J. Winzer, A. H. Gnauck, S. Chandrasekhar, S. Draving, J. Evangelista, and B. Zhu, "Generation and 1,200-km transmission of 448-Gb/s ETDM 56-Gbaud PDM 16-QAM using a single I/Q modulator," presented at the Eur. Conf. Exhib. Opt. Commun., Torino, Italy, Sep. 2010, Paper PDP 2.2.

[5] T. Kobayashi, A. Sano, A. Matsuura, Y. Miyamoto, and K. Ishihara, "Nonlinear tolerant long-haul WDM transmission over 1200 km using 538 Gb/s/ch PDM-64QAM SC-FDM signals with pilot tone," presented at the Opt. Fiber Commun. Conf. Expo./Nat. Fiber Opt. Eng. Conf., Los Angeles, CA, USA, Mar. 2012, Paper OM2A.5.

[6] H. Takahashi, K. Takeshima, I. Morita, and H. Tanaka, "400-Gbit/s Optical OFDM Transmission over 80 km in 50-GHz frequency grid," presented at the Eur. Conf. Exhib. Opt. Commun., Torino, Italy, Sep. 2010, Paper Tu.3.C.1.

[7] X. Zhou, L. E. Nelson, P. Magill, R. Isaac, B. Zhu, D. W. Peckham, P. Borel, and K. Carlson, "8×450-Gb/s, 50-GHz-spaced, PDM-32QAM transmission over 400 km and one 50 GHz-grid ROADM," presented at the Opt. Fiber Commun. Conf. Expo./Nat. Fiber Opt. Eng. Conf., Los Angeles, CA, USA, Mar. 2011, Paper PDPB3.

[8] X. Zhou, L. E. Nelson, P. Magill, R. Isaac, B. Zhu, D. W. Peckham, P. Borel, and K. Carlson, "1200 km transmission of 50 GHz spaced, 5×504-Gb/s PDM-32–64 hybrid QAM using electrical and optical spectral shaping," presented at the Opt. Fiber Commun. Conf. Expo./Nat. Fiber Opt. Eng. Conf., Los Angeles, CA, USA, Mar. 2012, Paper OM2A.2.

[9] X. Zhou, L. E. Nelson, P. Magill, R. Isaac, B. Zhu, D. W. Peckham, P. Borel, and K. Carlson, "High spectral efciency 400 Gb/s transmission using PDM time-domain hybrid 32–64 QAM and training-assisted carrier recovery," *J. Lightw. Technol.*, vol. 31, no. 7, pp. 999–1005, Apr. 1, 2013.

[10] X. Zhou, L. E. Nelson, P. Magill, R. Isaac, B. Zhu, D. W. Peckham, P. Borel, and K. Carlson, "12,000 km transmission of 100 GHz spaced, 8×495-Gb/s PDM time-domain hybrid QPSK-8QAM signals," presented at the Opt. Fiber Commun. Conf. Expo./Nat. Fiber Opt. Eng. Conf., Anaheim, CA, USA, Mar. 2013, Paper OTu2B.4.

[11] E. P. Silva, L. H. H. Carvalho, J. C. M. Diniz, J. R. Oliveira, V. B. Ribeiro, R. Silva, J. P. K. Perin, M. L. Silva, P. P. G. Cardoso, and J. Oliveira, "448 Gb/s dual-carrier PDM-RZ-16QAM on 75-GHz grid over 720 km with 10 flexi-grid ROADM passes," presented at the Latin Amer. Opt. Photon. Conf., Sao Sebastiao, Brazil, 2012, Paper LM1C.3.

[12] H. Zhang, J. X. Cai, H. G. Batshon, M. Mazurczyk, O. Sinkin, D. Foursa, Al. Pilipetskii, G. Mohs, and N. Bergano, "200 Gb/s and dual-wavelength 400 Gb/s transmission over transpacific distance at 6 b/s/Hz spectral efficiency," presented at the Opt. Fiber Commun. Conf. Expo./Nat. Fiber Opt. Eng. Conf., Anaheim, CA, USA, Mar. 2013, Paper PDP5A.6.

[13] W. R. Peng, I. Morita, and H. Tanaka, "Hybrid QAM transmission techniques for single-carrier ultra-dense WDM systems," presented at the OptoElectron. Commun. Conf., Kaohsiung, Taiwan, Jul. 2011, Paper 8D2–4.

[14] Q. Zhuge, X. Xu, M. Morsy-Osman, M. Chagnon, M. Qiu, and D. Plant, "Spectral efficiency-adaptive optical transmission using time domain hybrid QAM for agile optical networks," *J. Lightw. Technol.*, vol. 31, no. 15, pp. 2621–2628, Aug. 2013.

[15] H. Sun, R. Egorov, B. Basch, J. McNicol, and K. T. Wu, "Comparison of two modulation formats at spectral efficiency of 5 bits/dual-pol symbol," presented at the Eur. Conf. Exhib. Opt. Commun., London, U.K., Sep. 2013, Paper Th.2.D.3.

[16] H. Takahashi, I. Morita, and H. Tanaka, "The impact of the combined 8-QAM and QPSK subcarrier modulation for coherent optical OFDM," presented at the Opt. Fiber Commun. Conf. Expo./Nat. Fiber Opt. Eng. Conf., Los Angeles, CA, USA, Mar. 2011, Paper JWA30.

[17] R. Schmogrow, M. Winter, M. Meyer, D. Hillerkuss, A. Ludwig, B. Nebendahl, S. Ben-Ezra, J. Meyer, M. Dreschmann, M. Huebner, J. Becker, C. Koos, W. Freude, and J. Leuthold, "Real-time Nyquist pulse generation beyond 100 Gbit/s and its relation to OFDM," *Opt. Exp.*, vol. 20, no. 1, pp. 317–337, Dec. 2012.

[18] P. Bayvel, S. Kilmurray, and R. I. Killey, "Nonlinear transmission performance of digital Nyquist WDM and optical OFDM," in *Proc. 14th Int. Conf. Transparent Opt. Netw.*, Jul. 2012, pp. 1–4.

[19] R. Rios-Muller, J. Renaudier, O. Bertran-Pardo, A. Ghazisaeidi, P. Tran, G. Charlet, and S. Bigo, "Experimental comparison between hybrid-QPSK/8QAM and 4D-32SP-16QAM formats at 31.2 GBaud using Nyquist pulse shaping," presented at the Euro. Conf. Exhib. Opt. Commun., Amsterdam, The Netherlands, Sep. 2013, Paper Th.2.D.2.

[20] J. Leibrich and W. Rosenkranz, "Multidimensional constellations for power efficient and flexible optical networks," *IEEE Photon. Technol. Lett.*, vol. 26, no. 8, pp. 753–756, Apr. 2014.

[21] T. Inoue, N Saitama, and G. Satoh, "An international digital SNG transmission system with variable information/FEC coding rate control," *IEEE Global Telecommun. Conf.*, pp. 93–99, 1994.

[22] X. Zhou, L. E. Nelson, and P. D. Magill, "Rate-adaptable optics for next generation long-haul transport networks," *IEEE Commun. Mag.*, vol. 51, no. 3, pp. 41–49, Mar. 2013.

[23] M. Mazurczyk, "Spectral shaping for high spectral efficiency in long-haul optical transmission systems," presented at the Euro. Conf. Exhib. Opt. Commun., Amsterdam, The Netherlands, Sep. 2013, Paper Th.1.D.1.

[24] X. Zhou, J. Yu, M.-F. Huang, Y. Shao, T. Wang, L. E. Nelson, P. D. Magill, M. Birk, P. I. Borel, D. W. Peckham, and R. Lingle, "64-Tb/s, 8 b/s/Hz, PDM-36QAM transmission over 320 km using both pre- and post-transmission digital signal processing," *J. Lightw. Technol.*, vol. 29, no. 4, pp. 571–577, Feb. 15, 2011.

[25] J. Wang, C. Xie, and Z. Pan, "Reducing equalizer complexity in coherent receivers for Nyquist spectrally shaped systems with matched filters," presented at the Opt. Fiber Commun. Conf., Anaheim, CA, USA, Mar. 2013, Paper OTu2I.3.

[26] F. M. Gardner, "A BPSK/QPSK timing-error detector for sampled receivers," *IEEE Trans. Commun.*, vol. COM-34, no. 5, pp. 423–429, May 1986.

[27] M. Yan, Z. Tao, L. Dou, L. Li, Y. Zhao, T. Hoshida, and J. C. Rasmussen, "Digital clock recovery algorithm for Nyquist signal," presented at the Opt. Fiber Commun. Conf., Anaheim, CA, USA, Mar. 2013, Paper OTu2I.7.

[28] N. Stojanovic, C. Xie, Y. Zhao, B. Mao, and N. G. Gonzalez, "Modified gardner phase detector for Nyquist coherent optical transmission systems," presented at the Opt. Fiber Commun. Conf., Anaheim, CA, USA, Mar. 2013, Paper JTh2A.50.

[29] A. J. Viterbi and A. M. Viterbi, "Nonlinear estimation of PSK-modulated carrier phase with application to burst digital transmission," *IEEE Trans. Inf. Theory*, vol. IT-29, no. 4, pp. 543–551, Jul. 1983.

[30] T. Pfau, S. Hoffmann, and R. Noé, "Hardware-efficient coherent digital receiver concept with feed-forward carrier recovery for M-QAM constellations," *J. Lightw.. Technol.*, vol. 27, no. 8, pp. 989–999, Apr. 15, 2009.

[31] X. Zhou, "An improved feed-forward carrier recovery algorithm for coherent receiver with M-QAM modulation format," *IEEE Photon. Technol. Lett.*, vol. 22, no. 14, pp. 1051–1053, Jul. 15, 2010.

[32] X. Zhou and Y. Sun, "Low-complexity, blind phase recovery for coherent receivers using QAM modulation," presented at the Opt. Fiber Commun. Conf. Expo./Nat. Fiber Opt. Eng. Conf., Los Angeles, CA, USA, Mar. 2011, Paper OMJ3.

[33] J. G. Proakis, *Digital Communication*, 3rd ed. New York, NY, USA: McGraw-Hill, 1995.

[34] M. D. Feuer, L. E. Nelson, X. Zhou, S. L. Woodward, R. Isaac, B. Zhu, T. F. Taunay, M. Fishteyn, J. F. Fini, and M. F. Yan, "Joint digital signal processing receivers for spatial superchannels," *IEEE Photon. Technol. Lett.*, vol. 24, no. 21, pp. 1957–1960, Nov. 2012.

[35] X. Zhou and J. Yu, "Multi-level, multi-dimensional coding for high-speed and high spectral-efficiency optical transmission," *J. Lightw. Technol.*, vol. 27, no. 16, pp. 3641–3653, Aug. 2009.

[36] W. Shieh and K. P. Ho, "Equalization-enhanced phase noise for coherent-detection systems using electronic digital signal processing," *Opt. Exp.*, vol. 16, no. 20, pp. 15718–15727, 2008.

[37] C. Xie, "WDM coherent PDM-QPSK systems with and without inline optical dispersion compensation," *Opt. Exp.*, vol. 17, no. 6, pp. 4815–4823, Mar. 16, 2009.

[38] G. Colavolpe, T. Foggi, E. Forestieri, and M. Secondini, "Impact of phase noise and compensation techniques in coherent optical systems," *J. Lightw. Technol.*, vol. 29, no. 18, pp. 2790–2800, Sep. 2011.

Authors' biographies not available at the time of publication.